Effects of Multisine Signal Bandwidth on Eye Movement Dynamics

Büskens, Jasmijn; Pel, Johan J.M.; Pool, Daan M.

DOI
10.1016/j.ifacol.2019.12.112

Publication date
2019

Document Version
Final published version

Published in
IFAC-PapersOnline

Available online at www.sciencedirect.com

ScienceDirect

IFAC Papers Online CONFERENCE PAPER ARCHIVE

IFAC PapersOnLine 52-19 (2019) 282–287

Effects of Multisine Signal Bandwidth on Eye Movement Dynamics

Jasmijn Büskens,* Johan J.M. Pel and Daan M. Pool***

* *Control and Simulation Section, Aerospace Engineering, Delft University of Technology, Delft, The Netherlands (e-mail: d.m.pool@tudelft.nl).*

** *Vestibular and Oculomotor Research Group, Dept. of Neuroscience, Erasmus MC, Rotterdam, The Netherlands (e-mail: j.pel@erasmusmc.nl).*

Abstract: In the analysis of human motor skills, tracking tasks with multisine target signals are often performed as they allow for quantitative measurement, identification, and modeling of human control dynamics. In this paper, the same "*cybernetic*" approach is taken to analyze eye movement dynamics in *gaze* tracking tasks, where participants had to track a moving target marker across the screen) with their eyes (i.e., a eye-only task) and 2) with their dominant hand (i.e., a eye-hand task). A human-in-the-loop experiment with 10 participants was performed to measure the eye movement dynamics. These two different conditions were performed with four different bandwidths of the multisine target signal driving the movement of the visual stimulus. The results show that the measured eye movement dynamics can be identified from the data of all experiment conditions and can be accurately modeled as an underdamped mass-spring-damper system with a time delay. Furthermore, with increased target signal bandwidth the bandwidth of participants' eye movements also increases. Future development of gaze tracking tasks into a new tool for assessment of altered gaze behavior due to neurological diseases should take the balance between saccadic and smooth pursuit eye movements into account and avoid very high (i.e., too difficult) bandwidths to warrant accurate modelling of gaze dynamics.

Keywords: Eye movements, cybernetics, gaze dynamics, system identification, bandwidth

1. INTRODUCTION

The eyes are one of the most important sensory organs for humans. Processing visual information is the start of executing many daily tasks, e.g., handling or grabbing objects. During most of these tasks, the eyes precede the hands, e.g., grabbing an object or pointing somewhere. An important brain network is the visuomotor network to effectively process information into a goal-directed movement. Recent studies have indicated that multiple functional networks throughout the entire brain are already affected in early stage Alzheimer's and Parkinsons Disease (Seeley et al., 2009; Barber, 2010; Jellinger, 1991). Often these symptoms become apparent in the oculomotor system, thus affecting patients' eye movements (MacAskill and Anderson, 2016). Where low-level motor tasks exist to help diagnose diseases (Hoehn and Yahr, 1998; Goetz et al., 2007; Folstein et al., 1975; Dubois et al., 2000; Fahn S. and Elton R., 1987), more insight into the visuomotor network's properties in terms of timing, speed, and accuracy could help to catch early symptoms (De Boer et al., 2016).

Tracking tasks have been used extensively in investigations into human manual control behavior in a myriad of different tasks and scenarios (McRuer and Jex, 1967; Jones, 2014; Mulder et al., 2018). A tracking task is a task where a Human Controller (HC) continuously controls a system perturbed by a forcing function (e.g., multisine signal). Such a task also allows for using a "cybernetic approach" (Mulder et al., 2018), with which the HC's input-output behavior – i.e., the "control dynamics" – can be directly identified and quantified using mathematical (transfer function) models. In tracking tasks, HCs are known to adapt their control dynamics to the *bandwidth* of the forcing function signal, which is defined as the frequency up to which the signal has significant power.

To improve quantitative measurement of eye movement dynamics, this paper proposes to use the same "cybernetic" approach traditionally applied to human manual control behavior can be used to measure, identify, and model human gaze dynamics. For this a gaze tracking task was defined, where HCs track a moving visual stimulus on the screen with their eyes over a longer period of time, during which eye movements were recorded with an eye tracker. This approach allows for detailed identification and quantification of (degraded) smooth pursuit dynamics, but as is also the case for HC control dynamics (McRuer and Jex, 1967), the quality of the obtained results (i.e., the clinical relevance) strongly depends on the selected bandwidth of the presented visual stimulus. Furthermore, as being involved in manual tracking is known to affect eye movements (Niehorster and Siu, 2015), the possible interactions between the effects of signal bandwidth, eye movements, and hand tracking are of clear interest and have not been explicitly studied.

10.1016/j.ifacol.2019.12.112

In this paper, an experiment is described where ten representative participants performed a gaze tracking experiment while gaze data was recorded with a head-mounted video-based infrared eye-tracking system (EyeSeeCam (ESC) (EyeSeeTec, 2018)). Four different bandwidths of the multisine signal that was used to drive the visual stimulus, created by varying the number of high-amplitude low-frequency and low-amplitude high-frequency sines (McRuer and Jex, 1967), were tested. Furthermore, participants tracked all bandwidths under two conditions: eye-only tracking and eye-hand tracking of the same visual stimulus. Frequency response functions (FRFs) of the gaze dynamics, relating the lateral visual stimulus to recorded lateral gaze, were estimated from the experiment data. A transfer function model was fitted to the measured FRFs to quantify the differences in eye movement dynamics over the different experiment conditions.

2. METHODS

2.1 Task

Fig. 1 shows a schematic representation of the gaze tracking tasks performed in the experiment. The gaze tracking task was similar to a pursuit tracking task where the display presented continuous feedback of the visual stimulus, whose movement was defined by the target signal f_t, that was to be followed. While in traditional tracking tasks the focus is on the measured control inputs (u) of the HC, in the gaze tracking tasks considered in this paper we focus on how well the gaze signal g followed the visual stimulus. For this, the gaze dynamics $H_g(s)$ as shown in Fig. 1 were identified from measured input (f_t) and output (g) signals. While for the considered eye-only tracking tasks no hand data was collected, for the matching eye-hand tasks the traditional tracking task, indicated with the linear HC dynamics $H_p(s)$, the nonlinear human remnant signal n (McRuer and Jex, 1967), and the controlled dynamics $H_c(s)$ (here a simple gain), was also performed.

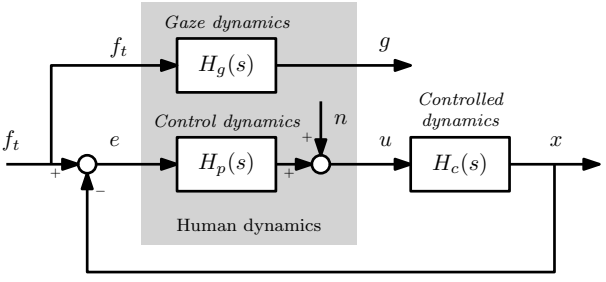

Fig. 1. Block diagram of the gaze tracking task.

2.2 Forcing Functions

To allow for estimating an FRF of the human gaze dynamics $H_g(s)$ (see Fig. 1) with an identification method based on Fourier coefficients, gaze tracking tasks with a multisine target forcing function were performed. The multisine f_t signal consisted of 11 sinusoids with frequencies ranging from 0.6-24 rad/s. This multisine target signal is given by:

$$f_t(t) = \sum_{k=1}^{N_t} A_t[k] \sin\left(\omega_t[k]t + \phi_t[k]\right) \qquad (1)$$

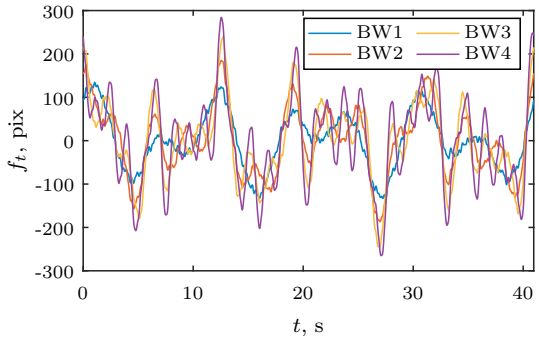

Fig. 2. Time responses of the four different target signals with increasing bandwidth (BW1-BW4).

In Eq. (1), the amplitude, frequency, and phase of the k^{th} sine in f_t are defined as $A_t[k]$, $\omega_t[k]$, $\phi_t[k]$, respectively. The considered frequencies and phases of the target signal are listed in Table 1. To avoid spectral leakage, f_t was composed of sinusoids with a period that fit an integer number of times in the measurement window of $T_m = 50$ s: e.g., $\omega_t[k] = 2\pi n_t[k]/T_m$ with $n_t[k]$ an integer. By varying the amplitude distribution $A_t[k]$, four different target functions were defined for the experiment with increasing *bandwidth* (BW), i.e., BW1 (lowest) to BW4 (highest). The distribution of the amplitudes in all four signals was determined using the same method as was used in (Wasicko et al., 1966; McRuer and Jex, 1967), that is, an augmented rectangular input spectrum with varying starting frequencies for the high-frequency reduced-amplitude shelve. The amplitudes in the high-frequency shelve were a factor 10 lower than those for the low-frequency sinusoids, see Table 1. Fig. 2 shows the time traces of the multisine signals with the four different bandwidth settings (BW1-BW4).

Table 1. Multisine signal parameters.

Target forcing function f_t							
k (-)	n_t (-)	ω_t (rad/s)	ϕ_t (rad)	$A_{t,1}$ (deg)	$A_{t,2}$ (deg)	$A_{t,3}$ (deg)	$A_{t,4}$ (deg)
1	4	0.614	7.239	0.75	0.75	0.75	0.75
2	7	1.074	0.506	0.75	0.75	0.75	0.75
3	11	1.994	7.860	0.075	0.75	0.75	0.75
4	17	2.915	8.1847	0.075	0.075	0.75	0.75
5	23	4.449	9.012	0.075	0.075	0.075	0.75
6	29	5.676	6.141	0.075	0.075	0.075	0.075
7	37	6.596	6.776	0.075	0.075	0.075	0.075
8	53	8.130	6.265	0.075	0.075	0.075	0.075
9	79	12.118	4.432	0.075	0.075	0.075	0.075
10	109	16.720	2.672	0.075	0.075	0.075	0.075
11	157	24.084	8.009	0.075	0.075	0.075	0.075

2.3 Apparatus

The experiment was performed at the vestibular and oculomotor research laboratory of the Department of Neuroscience, Erasmus MC Rotterdam. The test setup can be seen in Fig. 3. The setup included a chinrest on which the head was placed to limit head movements during the measurements and to ensure that the head was in the same position during different trials. The distance from the head to the screen was 0.5 m. Eye movements were measured with an EyeSeeCam eye tracker with a gaze accuracy <0.2

deg at 220 Hz, see also Fig. 4(a). The ESC was placed on the head of the participant positioned in front of the touchscreen. An example recorded image of the eye by the ESC is shown in Fig. 4(b). Finally, Fig. 3 also shows the touchscreen that was used to present the stimulus for the gaze tracking tasks, as well as for recording the hand inputs during the eye-hand condition trials. Hand inputs were provided in the right or left bottom corners of the screen (depending on which was the participant's dominant hand) on a blue bar that was shown, to avoid blocking the target marker with the hand and fingers.

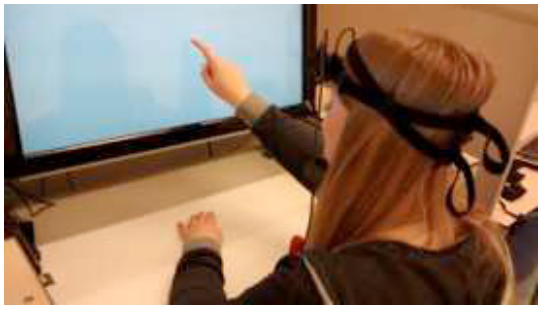

Fig. 3. Test setup for the gaze tracking tasks.

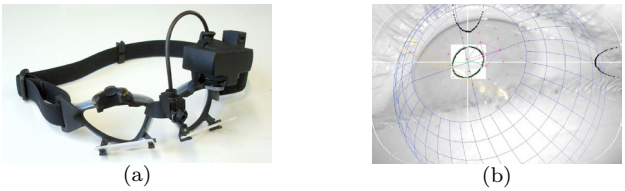

(a) (b)

Fig. 4. The EyeSeeCam (EyeSeeTec, 2018) (a) and an example of the recorded image of the eye (b).

The visual displays used for the eye-only and eye-hand conditions are shown in Fig. 5. In both cases, the blue circle with the cross represents the target signal f_t. For the eye-hand tasks, the red filled circle in Fig. 5(b) indicated the controlled element output x, see Fig. 1. For the eye-hand conditions, the participants were instructed to steer the red filled circle into the blue circle as accurately as possible. For the eye-only condition, the goal was to follow the blue circle as accurately as possible with the eyes. A cross was added to the blue circle to ensure that the subjects had a precise screen position to look and aim at.

2.4 Experiment Design

The design of the performed experiment is summarized in Table 2. Ten participants performed the experiment, all students from either the Erasmus MC or TU Delft. All participants performed all experiment conditions (within-subjects design) and performed three repeated trials of the eye-only tracking task and five repeated trials of the eye-hand tracking task for each stimulus bandwidth. Each trial had a duration of 50 s and each participant performed a total of 32 trials in the experiment.

2.5 Data Analysis

As is the case for any video-based eye-tracking system, the raw data from the EyeSeeCam contains gaps in the

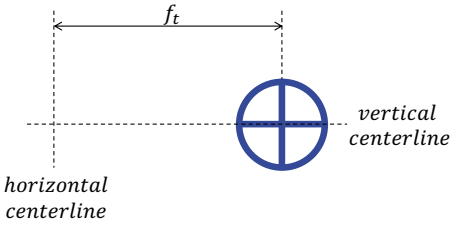

(a) Eye-only display.

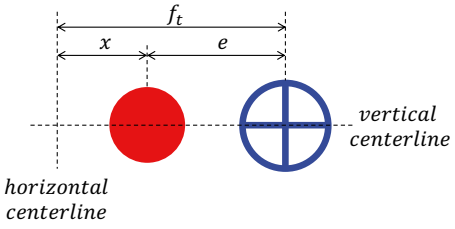

(b) Eye-hand display.

Fig. 5. Displays for the eye-only and eye-hand tasks.

data due to blinks. Blinks were detected for each recording and the blink data was replaced by interpolated values to ensure continuous signals for further analysis. Of the total number of performed repeated trials (i.e., 5 for eye-hand tracking and 3 for eye-only tracking, see Table 2) in general not all provided sufficiently reliable eye data. Only the trials that were deemed valid were used for identification of the gaze dynamics ($H_g(s)$ in Fig. 1) by estimating a gaze FRF according to:

$$\hat{H}_g(j\omega_t) = \frac{G(j\omega_t)}{F_t(j\omega_t)} \tag{2}$$

In Eq. (2), $G(j\omega_t)$ and $F_t(j\omega_t)$ indicate the Fourier transforms of the gaze (g) and target (f_t) signals, respectively, at the multisine stimulus frequencies ω_t. Based on the shape of the identified FRFs, the following four-parameter model was selected for modeling the gaze dynamics:

$$H_g(j\omega) = K_g e^{-j\omega\tau_g} \frac{\omega_g^2}{(j\omega)^2 + 2\zeta_g\omega_g j\omega + \omega_g^2} \tag{3}$$

The model of Eq. (3) represents an underdamped mass-spring-damper system with a gain K_g and time delay τ_g. This model was fitted to the estimated FRFs using a weighted complex least-squares cost function and a standard nonlinear optimizer (Matlab's `fminsearch` algorithm). The quality-of-fit of the obtained model fits was determined by calculating the models' Variance Accounted For (VAF), which expresses the accuracy with which the measured output signal (g) is replicated by the model as a percentage. Fig. 6 to 9 show representative examples of the estimated FRF (result of Eq. (2)), fitted model (Eq. (3)), and the quality of the modeled gaze signal for all four

Table 2. Experiment design.

Experiment	Bandwidths	Trials	Subjects	Total
Eye-hand tracking	4	5	10	200
Eye-only tracking	4	3	10	120
Total				320

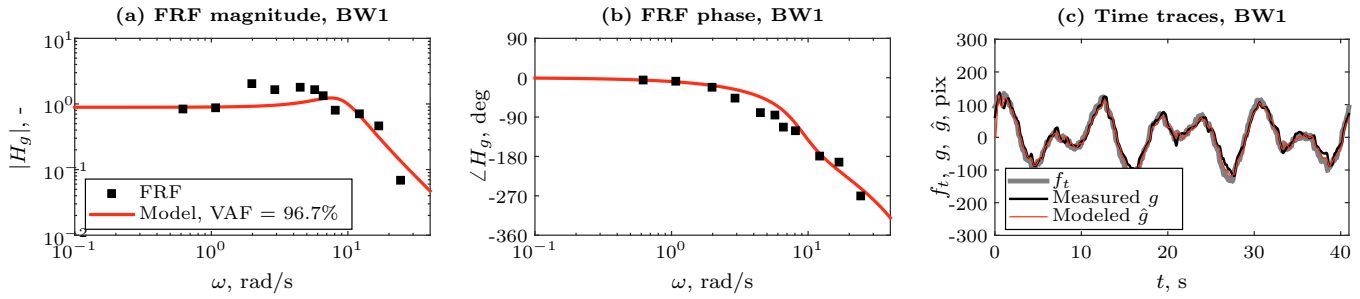

Fig. 6. Example gaze identification results for eye-only and BW1 (Subject 7).

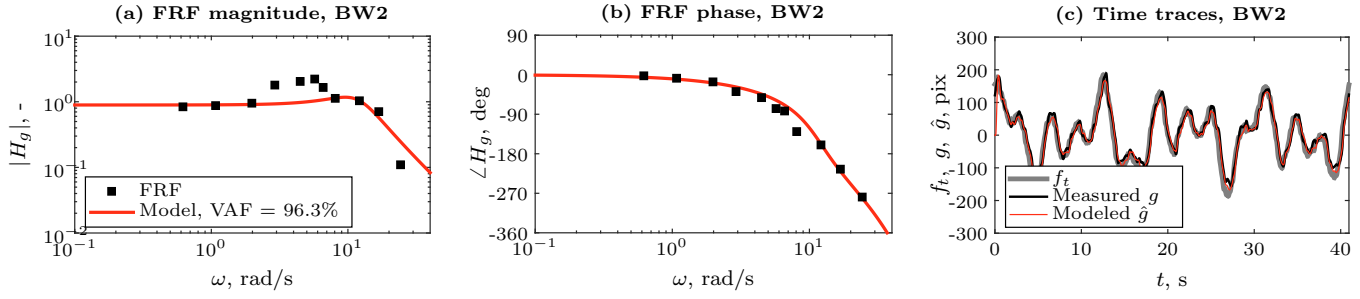

Fig. 7. Example gaze identification results for eye-only and BW2 (Subject 7).

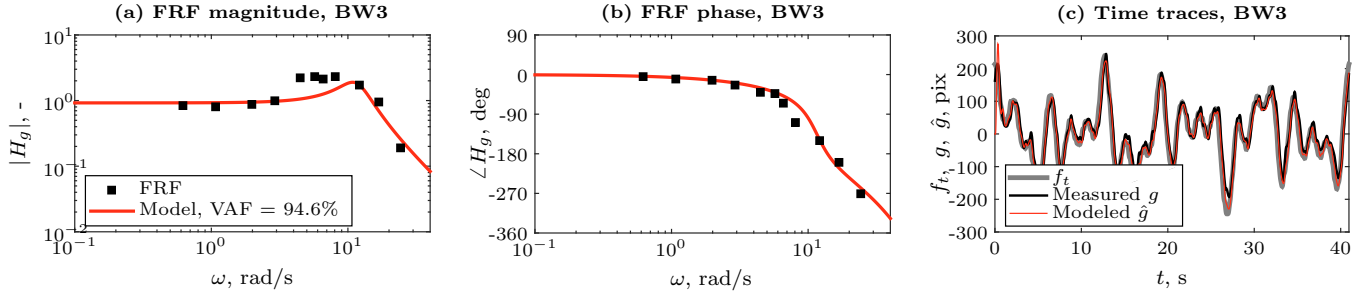

Fig. 8. Example gaze identification results for eye-only and BW3 (Subject 7).

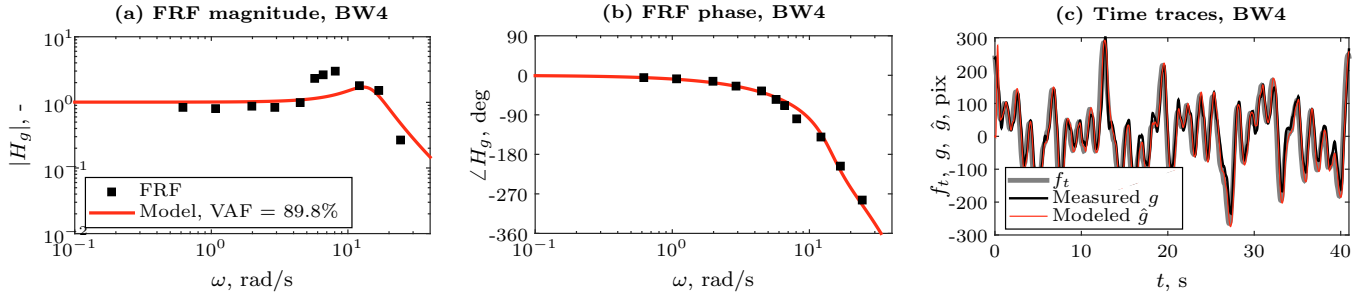

Fig. 9. Example gaze identification results for eye-only and BW4 (Subject 7).

bandwidths in the eye-only condition. Equivalent results were obtained for all other participants and experiment conditions. Overall, Fig. 6 to 9 show that the estimated gaze dynamics are consistent and that the proposed model accurately describes the measured gaze data with VAF values of around 90% or higher for all tested bandwidths.

3. RESULTS

3.1 Eye Movement Analysis

The eye movements that are recorded in the considered eye tracking task are a combination of both (catch-up) saccades (very fast eye movements where the eye quickly changes foveal viewpoint) and smooth pursuit eye movements, see Fig. 10(a). Saccades can be detected from their characteristic high eye velocities and accelerations. As is shown in Fig. 10(b), the eye's acceleration time trace shows saccades as a pair of two high-amplitude peaks in opposite directions, as eye velocity during a saccade is built up and stopped again almost instantaneously. For the collected data, saccades were detected by finding all acceleration peaks with a magnitude above 1000 pix/s^2, see black detection limits in Fig. 10(b).

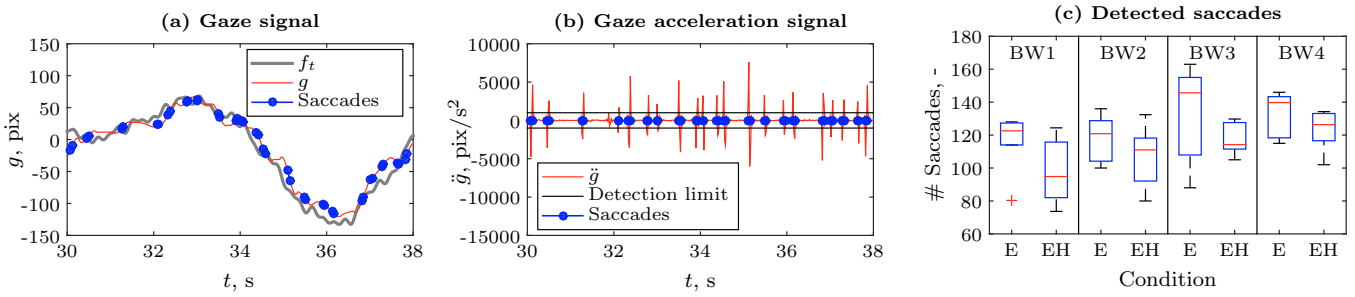

Fig. 10. Example of eye movement analysis and saccade detection. Gaze signal with detected saccades (a), gaze acceleration signal with used detection limit (b), and average detected saccades for each condition (c).

Fig. 10(c) shows the detected number of saccades for all participants and conditions. As increased signal bandwidth results in a movement trajectory that is more difficult to follow in smooth pursuit, increased numbers of saccades are expected with increasing bandwidth. For both the eye-only (E) and eye-hand (EH) tasks, Fig. 10(c) indeed shows increased occurrence of saccades for BW3 and BW4 compared to BW1 and BW2. Furthermore, Fig. 10(c) shows that when the signal is also tracked with the hand (EH) on average between 20-30 less saccades occur, hence resulting in smoother eye movements, which is consistent with (Niehorster and Siu, 2015).

3.2 Gaze Identification and Modeling

For modeling the gaze dynamics, the entire gaze signal g as shown in Fig. 10(a) was used, i.e., the detected saccades were not removed. This was done for two reasons: 1) to allow for fairer comparison of the different bandwidth conditions (Fig. 10(c) shows that more saccades and hence more distance traveled by the eye would be removed for higher BWs) and 2) to avoid non-smooth signal transitions for the frequency-domain identification approach, i.e., Eq. (2). As illustrated in Fig. 6 to 9 for a single subject, the gaze dynamics model of Eq. (3) was fitted to an estimated FRF of $H_g(j\omega)$ for every participant and experiment condition.

Fig. 11 shows the overall quality-of-fit of the fitted gaze models, expressed in terms of the Variance Accounted For (VAF). As can be seen in Fig. 11, on average VAF values between 80-95% were obtained. The VAF values are seen to decrease with increasing bandwidth, which indicates that the linear model of Eq. (3) was less accurate with increasing bandwidth. Furthermore, especially for BW3 and BW4, higher VAF values are found for the eye-hand tasks than for the eye-only conditions. Both findings are consistent with the saccade count data of Fig. 10(c) and suggests that our proposed approach to modeling the gaze dynamics is less accurate with more frequent saccades.

Fig. 12 shows the estimated parameters of the gaze model of Eq. (3), i.e., the gain K_g, the delay τ_g, the natural frequency ω_g, and the damping ratio ζ_g. For the gaze gain K_g, Fig. 12(a) shows values close to unity for the low bandwidths, as expected for accurate following of the target marker. Furthermore, K_g is seen to decrease with increased bandwidth as well as when also tracking with the finger (EH conditions), indicating that participants did not follow the full amplitude of the f_t signal across the screen on average. For the gaze delay (see Fig. 12(b)) no consistent variation across conditions was observed,

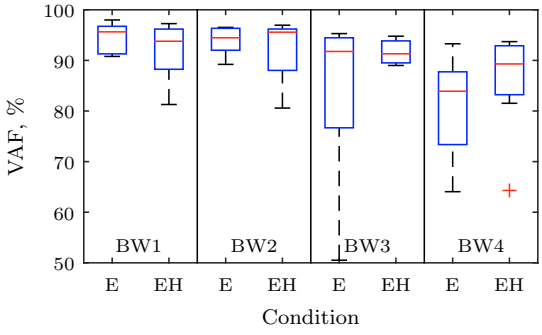

Fig. 11. Fitted gaze model Variance Accounted For (VAF).

i.e., τ_g values of on average between 0.1 and 0.3 s were measured. Fig. 12(c) shows a clear increase in ω_g, from around 10 rad/s for BW1 to 12 rad/s for BW4 on average, which indicates an adapted higher "bandwidth" of the gaze dynamics. Finally, for ζ_g Fig. 12(d) shows a slight reduction with increasing bandwidth, as well as a slight increase from E to EH conditions (except for BW4). Overall, the results in Fig. 12 indicate that with increasing bandwidth, the gaze dynamics show considerable adaptation, characterized by a reduced gain (less accurate tracking of stimulus amplitude) and a higher "bandwidth" (more accurate high-frequency tracking).

4. CONCLUSIONS

This paper presents the results of a gaze tracking experiment in healthy participants. Variations in eye movement dynamics with four different bandwidths of the visual (multisine) stimulus were assessed for eye-only tracking (E) and eye-hand tracking (EH) conditions. The measured gaze dynamics were analyzed with frequency-domain identification techniques and modeled with a four-parameter transfer function model. Consistent with literature, the analysis of the measured gaze signals showed increased number of catch-up saccades with increasing signal bandwidth, in addition to a lower saccade count (i.e., smoother eye movements) when also tracking the stimulus with the hand (EH conditions). From the obtained gaze identification results it was found that the proposed methodology results in highly accurate (i.e., VAF $>$ 80%) modeling of the measured gaze signals. Furthermore, the estimated gaze model parameters showed clear adaptation of the gaze dynamics to increased bandwidth, which resulted less accurate tracking of the full stimulus amplitude (reduced K_g), but increased high-frequency bandwidth (increased

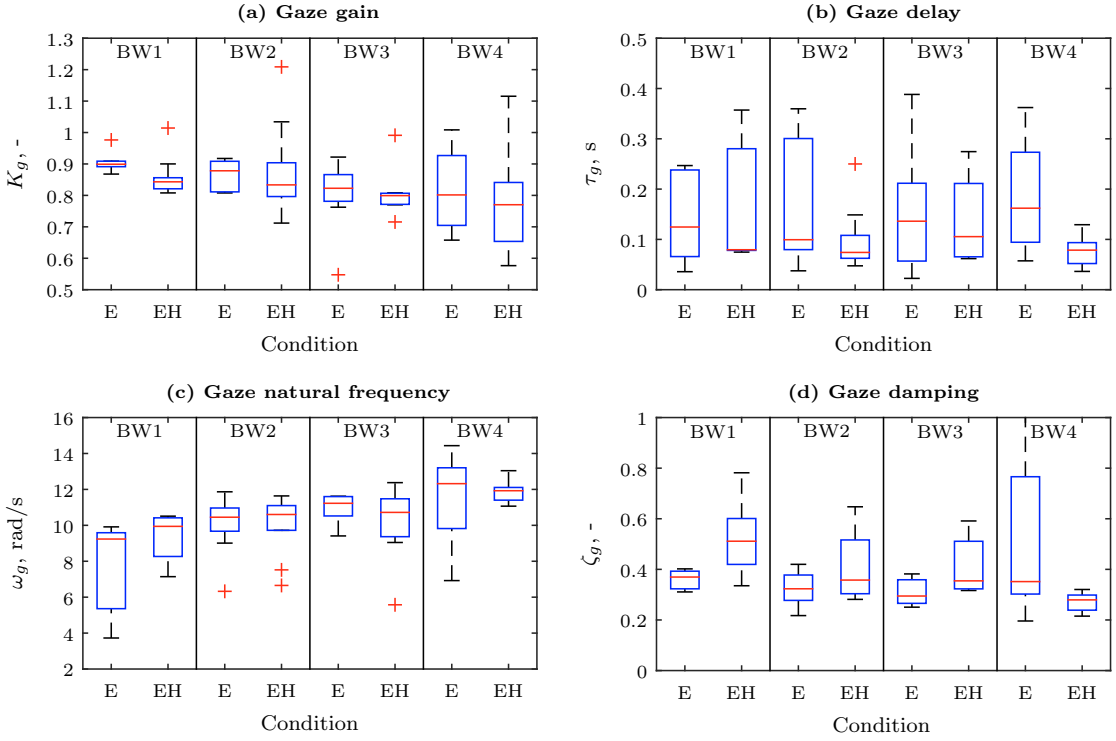

Fig. 12. Estimated gaze model parameters.

ω_g). Future development of gaze tracking tasks into a new tool for assessing altered gaze behavior due to aging or neurological diseases should take the balance between saccadic and smooth pursuit eye movements into account and avoid very high (i.e., too difficult) bandwidths to warrant accurate modelling of gaze dynamics.

REFERENCES

Barber, R.C. (2010). Biomarkers for early detection of alzheimer disease. *J. of the American Osteopathic Assoc.*, 110(9), S10–5.

De Boer, C., Van der Steen, J., Mattace-Raso, F., Boon, A.J., and Pel, J.J. (2016). The Effect of Neurodegeneration on Visuomotor Behavior in Alzheimer's Disease and Parkinson's Disease. *Motor Control*, 20(1), 1–20.

Dubois, B., Slachevsky, A., Litvan, I., and Pillon, B. (2000). The FAB: a Frontal Assessment Battery at bedside. *Neurology*, 55(11), 1621–6.

EyeSeeTec (2018). EyeSeeCam vHIT. URL `https://www.eyeseetec.de/`. Visited: 18/12/2018.

Fahn S. and Elton R. (1987). Unified Parkinson's Disease Rating Scale. *Recent Developments in Parkinson's Disease*, 2, 153–163.

Folstein, M.F., Folstein, S.E., and McHugh, P.R. (1975). Mini-mental state. A practical method for grading the cognitive state of patients for the clinician. *Journal of psychiatric research*, 12(3), 189–98.

Goetz, C.G., Fahn, S., Martinez-Martin, P., Poewe, W., Sampaio, C., Stebbins, G.T., Stern, M.B., Tilley, B.C., Dodel, R., Dubois, B., Holloway, R., Jankovic, J., Kulisevsky, J., Lang, A.E., Lees, A., Leurgans, S., LeWitt, P.A., Nyenhuis, D., Olanow, C.W., Rascol, O., Schrag, A., Teresi, J.A., Van Hilten, J.J., and LaPelle, N. (2007). Movement Disorder Society-sponsored revision of the Unified Parkinson's Disease Rating Scale (MDS-UPDRS): Process, format, and clinimetric testing plan. *Movement Disorders*, 22(1), 41–47.

Hoehn, M.M. and Yahr, M.D. (1998). Parkinsonism: onset, progression, and mortality. *Neurol.*, 50(2), 318–334.

Jellinger, K.A. (1991). Pathology of Parkinsons disease. *Molecular and Chemical Neuropathol.*, 14(3), 153–197.

Jones, R.D. (2014). Measurement and Analysis of Sensory-Motor Performance: Tracking Tasks. In *Medical Devices and Human Engineering*. CRC Press LLC.

MacAskill, M.R. and Anderson, T.J. (2016). Eye movements in neurodegenerative diseases. *Current Opinion in Neurology*, 29(1), 61–68.

McRuer, D.T. and Jex, H.R. (1967). A Review of Quasi-Linear Pilot Models. *IEEE Transactions on Human Factors in Electronics*, HFE-8(3), 231–249.

Mulder, M., Pool, D.M., Abbink, D.A., Boer, E.R., Zaal, P.M.T., Drop, F.M., van der El, K., and van Paassen, M.M. (2018). Manual Control Cybernetics: State-of-the-Art and Current Trends. *IEEE Transactions on Human-Machine Systems*, 48(5), 468–485.

Niehorster, D.C. and Siu, W.W.F. (2015). Manual tracking enhances smooth pursuit eye movements. *Journal of Vision*, 15(2015), 1–14. doi:10.1167/15.15.11.doi.

Seeley, W.W., Crawford, R.K., Zhou, J., Miller, B.L., and Greicius, M.D. (2009). Neurodegenerative diseases target large-scale human brain networks. *Neuron*, 62(1), 42–52.

Wasicko, R.J., McRuer, D.T., and Magdaleno, R.E. (1966). Human Pilot Dynamic Response in Single-loop Systems with Compensatory and Pursuit Displays. Technical Report AFFDL-TR-66-137, Air Force Flight Dynamics Laboratory.